# Topological Anderson phases in heat transport

He Gao[1,4], Guoqiang Xu[2,4,*], Xue Zhou[2,3], Shuihua Yang[2], Zhongqing Su[1,*] Cheng-Wei Qiu[2,*]

[1] Department of Mechanical Engineering, The Hong Kong Polytechnic University, Hung Hom, Kowloon, Hong Kong SAR, China.

[2] Department of Electrical and Computer Engineering, National University of Singapore, Kent Ridge, Singapore.

[3] School of Computer Science and Information Engineering, Chongqing Technology and Business University, Chongqing, China.

[4] These authors contributed equally to this work.
Email: xu_gq@nus.edu.sg; zhongqing.su@polyu.edu.hk; chengwei.qiu@nus.edu.sg.

## Abstract

Topological Anderson phases (TAPs) offer intriguing transitions from ordered to disordered systems in photonics and acoustics. However, achieving these transitions often involves cumbersome structural modifications to introduce disorders in parameters, leading to limitations in flexible tuning of topological properties and real-space control of TAPs. Here, we exploit disordered convective perturbations in a fixed heat transport system. Continuously tunable disorder-topology interactions are enabled in thermal dissipation through irregular convective lattices. In the presence of a weak convective disorder, the trivial diffusive system undergos topological Anderson phase transition, characterized by the emergence of topologically protected corner modes. Further increasing the strength of convective perturbations, a second phase transition occurs converting from TAP to Anderson phase. Our work elucidates the pivotal role of disorders in topological heat transport and provides a novel recipe for manipulating thermal behaviors in diverse topological platforms.

Keywords: topological Anderson insulator, non-Hermitian disorder, topological phase transition, heat transport

## 1. Introduction

Topological insulators (TIs) are known for their nontrivial boundary states [1-9], which arise as a consequence of the non-trivial topology of the material's electronic structure. The generalization of the conventional TIs into higher dimensions gives rise to more exotic topological features, leading to the emergence of the gapless lower-dimensional boundary states [10-19], which are typically robust against certain types of distortions, but vulnerable to strong disorders due to Anderson localization (AI) [20]. Recent explorations have uncovered an intriguing phenomenon:certain disorder configurations may induce topological phase transitions instead of inhibiting them, known as topological Anderson insulator (TAI) [21-25]. This concept is initially demonstrated in Hermitian systems, including cold atomic wires [26], electric circuit [27], phononic and photonic crystals [28-31], where disorders are introduced by modifying the onsite potentials or coupling strengths. More recently, this concept is generalized to non-Hermitian systems, where the rich interactions of disorder, non-Hermiticity and topology give rise to the production of non-Hermitian TAIs [32-36]. By strategically manipulating and introducing a global non-Hermitian disorder configuration to initially ordered structures, the topological phase transition can be induced, which has been successfully observed in quantum dynamics [37] and classical wave systems [38,39]. However, achieving these transitions often necessitates structural modifications, limiting the flexibility in tuning topological properties.

The extension of non-Hermitian physics and topological insulating phases into diffusive contexts raises the new territory of topological heat transport in both skew-Hermitian system and non-Hermitian system [40-48]. These discoveries reveal the nontrivial states and exotic behaviors, such as dynamic encircling exceptional points [49], Weyl exceptional

rings [50], and edge states [51,52]. The recent discoveries further reveal significantly hierarchical states in both non-Hermitian diffusive quadrupole topological insulator [53] through real-space modifications and advective flexibility and skew-Hermitian 2D SSH heat conduction system [54]. Nevertheless, all state-of-the-art studies only focus on the well-organized structure and configurations of the thermal couplings and advections. Such strategies lead to the forced efforts on the diffusive evolution, and result in the ordered field distributions towards bias evolutive direction with significant local entropy reduction instead of disordered regime [figure 1(a)]. Thus, a curious question raises whether an approximate system to the natural evolution with disordered or partial random [figure 1(b)] exists to support the topologically nontrivial states in diffusive contexts. Unfortunately, in the realm of diffusive heat transport, the exploration of inducing ordered field distributions in random heat transport remains unexplored.

In this work, we conduct a comprehensive investigation into the pivotal role of Hermitian disorders in thermal topological systems. In the context of dissipative diffusion, the relevant Hamiltonian, in the absence of any disorders, is skew-Hermitian in nature, meaning the Hamiltonian matrix is purely imaginary. Importantly, if disorders are introduced in the dissipative diffusion system, these added disorders will be Hermitian, in contrast to the underlying skew-Hermitian Hamiltonian. We establish two thermal convective systems, each representing trivial and nontrivial topological phases. By manipulating the Hermitian disorder configurations, with on-site convections, the topological phases can be flexibly switched. In the case of the trivial system, as the disorder strength is increased, the system transforms from a trivial state into a higher-order TAI [25,36,55], and then further into an Anderson insulator (AI) with stronger disorder. On the other hand, the in-gap topological corner modes in the nontrivial lattice persist for a weak disorder strength. The phase transition in the nontrivial lattice would be induced by further increasing the disorder strength. Numerical predictions and experimental demonstrations depict the evolution of the temperature field with varying non-Hermitian disorder strength. Our work uncovers the intricate interplay between Hermitian disorders and topology in thermal systems, bridging the gap between random and ordered heat diffusion. Moreover, our findings pave the way for the exploration of disorder-induced topological phenomena in various diffusion processes.

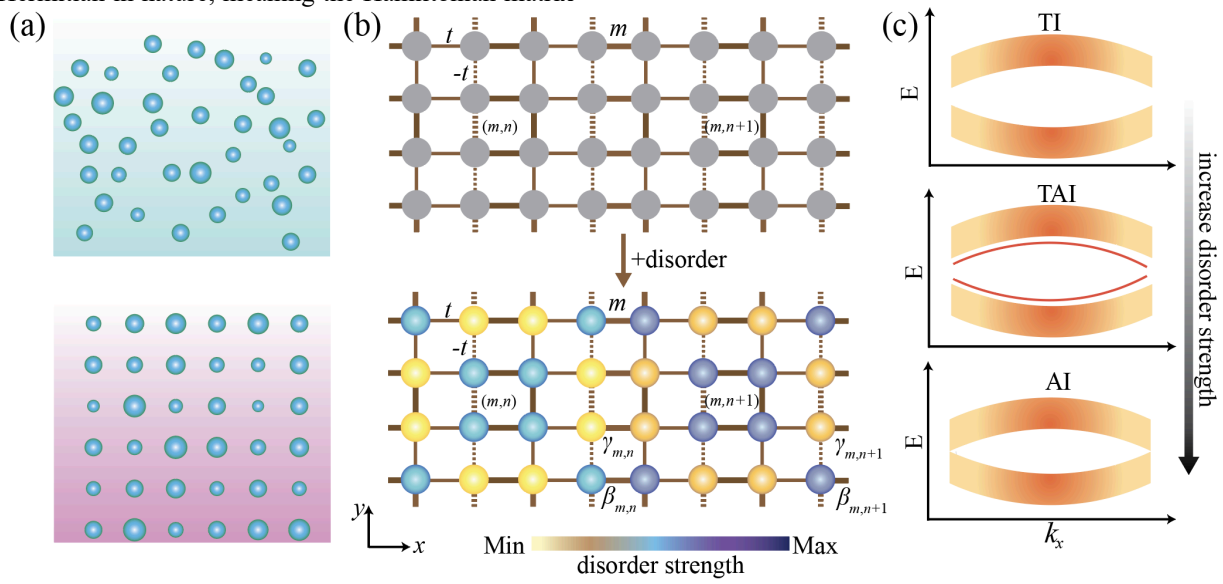


**Figure 1. Conceptual illustration of the non-Hermitian TAI.** (a) The upper and lower panels illustrate the disordered and partially ordered particles, respectively. (b) Tight-binding models of the topological lattices without non-Hermitian disorders (upper panel) and with non-Hermitian disorders (lower panel). The entire lattice comprises $4M\times4N$ atoms. In the lower panel, the colors for each atom denote the strength of the on-site non-Hermitian disorder. The solid and dashed lines present the positive and negative couplings, respectively. (c) The evolution of the band structures with the increase of non-Hermitian disorder strength. In the calculations, the $x$ and $y$ boundaries are set to be periodic and open, respectively.

## 2. Topological Anderson phases

To demonstrate the idea, we consider a modified non-Hermitian Benalcazar–Bernevig–Hughes (BBH)

model, which is based on the Hermitian BBH model. The Hamiltonian of the Hermitian BBH model in momentum space is described as

$$H = \begin{bmatrix} 0 & t+me^{-ik_x} & t+me^{ik_y} & 0 \\ t+me^{ik_x} & 0 & 0 & -t-me^{ik_y} \\ t+me^{-ik_y} & 0 & 0 & t+me^{-ik_x} \\ 0 & -t-me^{-ik_y} & t+me^{ik_x} & 0 \end{bmatrix} \quad (1)$$

where $t$ and $m$ present the intracell and intercell coupling strengths, respectively. For the modified non-Hermitian BBH model, as illustrated in the lower panel of figure 1(b), the Hamiltonian in real space can be written as

$$H = \sum_{pq} t_{pq}\, e^{i\phi_{pq}} c_p^{\dagger} c_q + \sum_p i\delta_p\, c_p^{\dagger} c_p \quad (2)$$

where $t_{pq}$ presents the nearest-neighbor coupling strength between sites $p$ and $q$. $\phi_{pq}$ is designed to be $\pi(0)$ for the couplings denoted by the dashed (solid) lines in figure 1(b). $t_{pq}$ is set to be $t$ or $m$ for the couplings between different sites, indicated by the thin and thick lines, respectively. $\delta_p$ indicates the onsite non-Hermitian disorder, which is set to be $\gamma_{m,n}$ and $\beta_{m,n}$ ($m$=1⋯$M$, $n$=1⋯$N$) for the sites with different colors. The non-Hermitian parameters, denoted by $\gamma_{m,n}$ and $\beta_{m,n}$, are uniformly distributed in the interval [-0.5$W$, 0] and [-1.5$W$, -$W$], respectively, where $W$ represents the disorder strength and plays a crucial role in inducing topological phase transitions. This non-Hermitian disorder configuration leads to an unequally effective reduction of coupling strengths between different sites. For example, in a trivial lattice ($t$>$m$) subjected to periodic (open) boundary condition in $x$ ($y$) direction, the addition of non-Hermitian disorders gradually closes and reopens the initially opened bandgap [upper panel of figure 1(c)], accompanying with the emergence of in-gap boundary modes [indicated by the red lines in the middle panel of figure 1(c)], resulting in a TAI. As $W$ is further strengthened, the bandgap closes once again, leading to the transformation of the system into an AI, as illustrated in the lower panel of figure 1(c). In the calculations of figure 1(c), the on-site non-Hermitian terms along $y$ direction are assumed to be disordered, while those along $x$ direction are uniform.

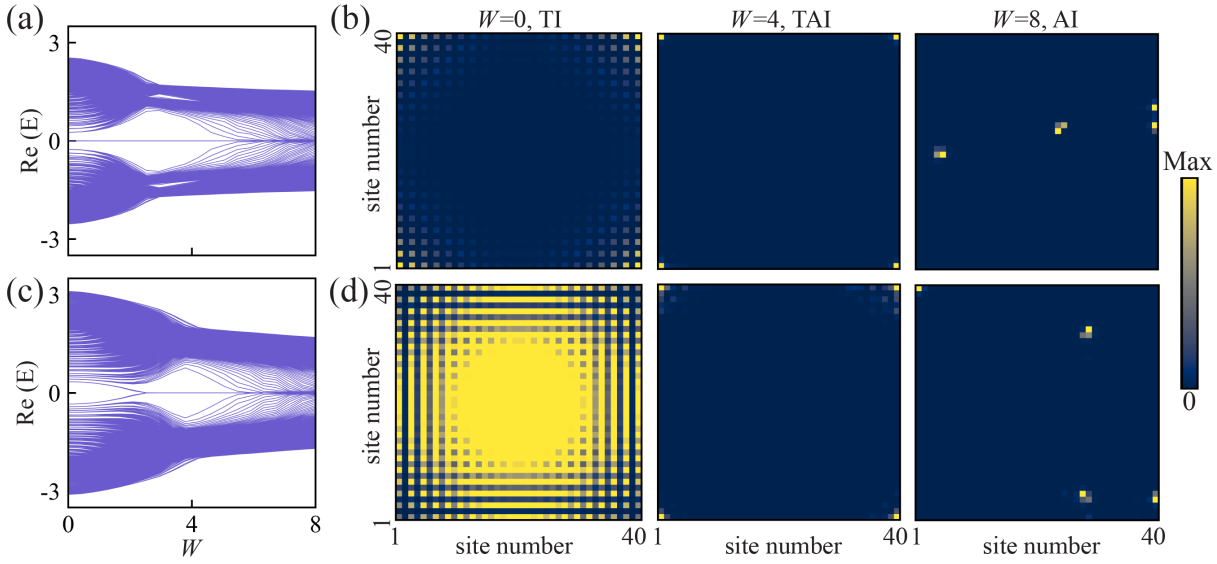


**Figure 2. Calculations for the 2D tight-binding model.** The averaged real parts of the eigenvalue with the evolution of non-Hermitian disorders $W$ for a finite lattice with open boundary conditions under (a) $t$=0.8 and (c) $t$=1.2, respectively. Averaged intensity profiles of the four eigenmodes around zero energy fonor a finite lattice under (b) $t$=0.8 and (d) $t$=1.2, respectively. In panels (b) and (d), the results for the lattice are presented from left to right, corresponding to $W$=0, $W$=4, and $W$=8, respectively. In all calculations, the lattice is composed of 40×40 elements, and the coupling strength $m$ is fixed to be 1. All the calculations are averaged over 50 disorder configurations.

To investigate the effects of introducing non-Hermitian disorders, we calculate the averaged eigenvalue profile with the evolution of $W$ for 50 disorder configurations under different coupling parameters. Here, two finite lattices with 40×40 sites are considered. As $t$ = 0.8 and $m$ = 1, a nontrivial bandgap with four degenerated corner modes exists when $W$ = 0, as presented in figure 2(a). The total intensity field for these four zero eigenmodes is given in the left panel of figure 2(b), clearly illustrating the localization of power at the four corners. Through a gradual introduction of non-Hermitian disorders, the bandgap gradually widens while the zero corner modes persist [figure 2(a)]. In the middle panel of

figure 2(b), we plotted the eigenstate profile for the four zero modes at $W = 4$. A comparison with the left panel of figure 2(b) reveals a more significant localization of power at the corners, attributable to the increased bandgap width. As $W$ exceeds 4, the bandgap begins to narrow [figure 2(a)], and it eventually closes when $W>5$, making the topological phase transition into the AI phase. At $W=8$, within this AI region, we find that the energy becomes trapped at several positions throughout the lattice, as demonstrated by the calculated eigenmode around the zero energy in the right panel of figure 2(b).

Interestingly, the presence of non-Hermitian disorder can induce a nontrivial behavior even in a trivial system ($t = 1.2$ and $m = 1$). As demonstrated in figure 2(c), without the non-Hermitian disorders, there are no corner modes in the bandgap, which is further confirmed by the calculated eigenmodes shown in the left panel of figure 2(d). Surprisingly, when introducing the non-Hermitian disorder and strengthening $W$, four modes gradually evolve from the bulk bands into the zero corner modes, and at the same time the topological phase transition is produced. This transition can also be clearly distinguished by comparing the eigenstates in figure 2(d), where the bulk mode in the left panel is transformed to the corner mode in the middle panel. The calculated density of states provides further confirmation of the non-Hermitian disorder-induced topological modes, as presented in the supplementary material. These non-Hermitian disorder-induced topological corner modes also exhibit robustness against randomly both Hermitian and non-Hermitian disorders (details see supplementary material).

By further increasing $W$, the bandgap gradually expands, and finally closes when $W$ is around 5.5, as depicted in figure 2(c). The closure of the bandgap is accompanied by a second phase transition, leading the system to become AI. In this regime, power localization occurs at some specific positions within the bulk of the lattice, as presented in the right panel of figure 2(d). The topological phases of these disordered systems can be characterized by calculating the quadrupole moment. The quadrupole moment is quantized due to the presence of pseudo-anti-Hermiticity symmetry, given by the relation:

$$H = -\eta H^{\dagger} \eta \qquad (3)$$

where $\eta$ is a diagonal matrix with the odd (even) diagonal atom being 1 (-1). In the topological nontrivial (trivial) system, the quadrupole moment is quantized to be 0.5 (0). The detailed calculations can be found in the supplementary material.

## 3. Phase transitions in heat transport

Then, the convective systems consisting of 16 sites for holding electromagnetic fluid both along the $x$ and $y$ directions [figure 3(a)] are proposed to manifest these topological Anderson phases. It is worth to note that the thermal coupling strength can be tuned by changing the heat exchange area under the same heat input [53].

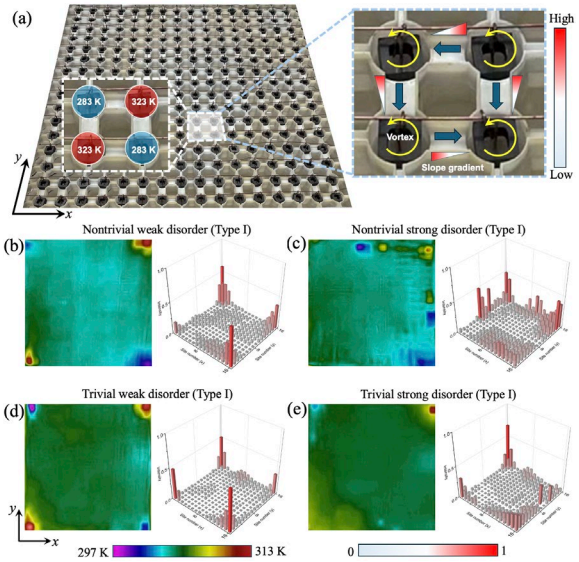


**Figure 3. TAPs of the convective system.** (a) Experimental setup for the convective system for supporting the TAP under different advective Hermiticities. The left insert present the heating strategy with alternative heating and cooling sources in each four-site unit. The positive and negative couplings are achieved by fabricating slope gradients with different orientations in the coupling channels. The fluid is motivated by the Lorentz force provided by external electromagnetic fields. The black blocks and pillars are electrodes and magnets are imposed to the bottom of each site. (b)-(e), The temperature and field intensity profile of the nontrivial and trivial cases respectively under weak and strong disorders (Type I). Among them, (b) and (c) indicate the nontrivial cases under weak and strong disorders. (d) and (e) are the trivial cases under weak and strong disorder advective configurations. In (b)-(e), the left and right insets present the temperature and field intensity, respectively. All the disorder configurations are given in the supplementary material.

In that case, we can correspondingly adjust the widths of the intercell and intracell fluid channels to satisfy the nontrivial and trivial phases. For simplification and generalization, we fix the width of the intercell fluid channel ($m$=1) and motivate the width of the intracell ones ($t$ = 0.8, 1.2). In diffusive systems, the Hamiltonian exhibits a skew-Hermitian relation, so that the introduced advections serve as

analogs of real Hermitian operators, representing the gain and loss in classical wave systems. In order to create the disorder in the Hermiticities, we adopt differentiated advections to each site (fluid pools) via modulating the Lorentz force imposed by corresponding voltages. In that case, the Hermitian advection in each site can be manipulated independently thus resulting in the disorder distributions of the convective amplitudes.

We first implement the nontrivial case ($t$ = 0.8, $m$ = 1) with a weak degree of disorder ($W$ = 4) and capture the temperature profile. As presented in figure 3(b), significant corner modes with apparently high/low temperatures are observed at the four corners of the entire sample, while the temperature fields of the other sites are rapidly homogenized. Further tracking the field intensity of the temperature distribution with the normalized value $I = \left|\frac{(T^* - \bar{T}_{mea})}{\Delta T_{mea}}\right|$, where $T^*$, $\bar{T}_{mea}$ and $\Delta T_{mea}$ respectively denote the target temperature at specific measured points, the average temperature of the system, and the difference between the highest temperature and $\bar{T}_{mea}$ at the measured moments [53], the intensities of the four corners indicate larger values in stark contrast to the other positions, thus revealing the emerging corner states with energy localizations. Upon further increasing the disorder to strong regime ($W$ = 8), the system undergoes a transition to be AI, as predicted in figure 2(b). In this scenario, bound states are observed to emerge on specific sites, extending beyond just the corners of the system, due to the appearance of Anderson localization. Moreover, the introduced disorder plays a crucial role in driving the transitions from a trivial system to TAI and AI, as depicted in figure 2(c). To validate these phenomena, we systematically introduce weak and strong degrees of disorder to the initially trivial convective system ($t$=1.2, $m$=1). Under weak disorder condition ($W$ = 4), significant localized states appear at the corners, confirming the successful transition to a TAI [figure 3(d)]. Further increasing the degree of disorder to $W$ = 8, energy localizations still exist, not only at the corners but also at other sites within the system, indicating a transition to an AI [figure 3(e)].

Note that, in all the experimental demonstrations, we adopt the thermal source configuration with a temperature range of 40 K at the initial states [figure 3(a)] to act as the typical quadrupole distributions in electrostatics. Then, we actuate the entire system with tailored advections of each site and remove the heating and cooling sources to measure the behaviors at steady states after the natural evolution of the thermal fields. The final measured temperature range is 16 K.

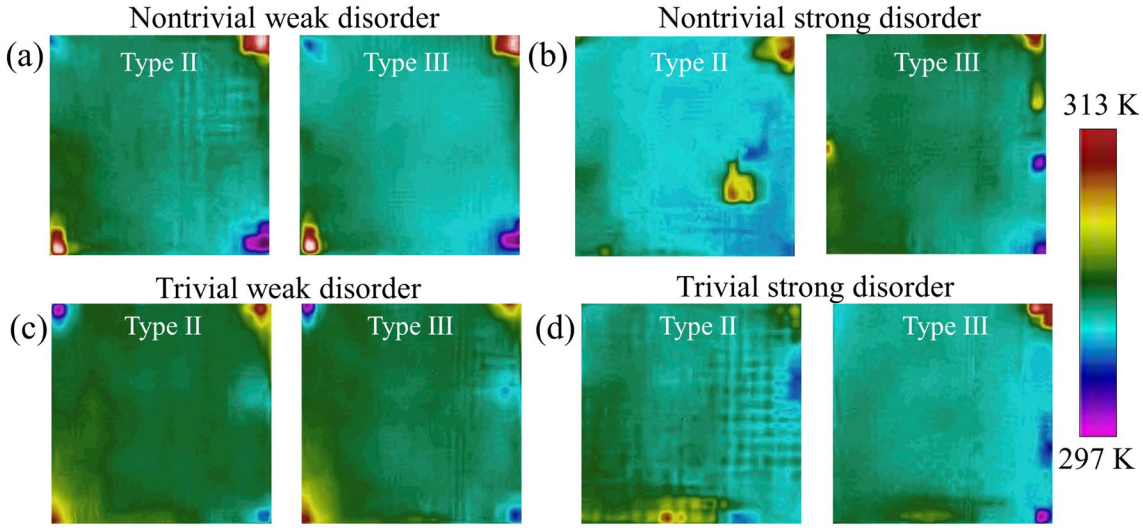


**Figure 4. The bound states under different disorder configurations.** The measured temperature fields of the nontrivial systems under different disorder patterns (Type II and Type III) for the (a) weak and (b) strong degrees of disorders, respectively. The measured temperature fields of the trivial systems under different disorder patterns (Type II and Type III) for the (c) weak and (d) strong degrees of disorders, respectively.

As demonstrated above, the transitions from nontrivial/trivial cases to TAIs and AIs can be achieved by introducing tailored Hermitian advective disorder on each site, following a specific configuration. In order to investigate the robustness of these bound states, we vary the configurations of the disorder patterns (figure 4) while maintaining the same degrees of disorder ($W$ = 4 and 8) as shown in figure 3. For both the nontrivial and trivial cases, we design two additional disorder configurations (Type II and Type III), which are applied to the same convective system as shown in figure 3(a). These three types of disorder

profiles (including the previously studied Type I) are all generated using random numbers uniformly distributed within the same predefined intervals (details are presented in the supplementary material). which are used to demonstrate that the results are not accident. These studies aim to demonstrate that the observed results are regardless of the specific disorder profile type. By analyzing the temperature fields, we observe that the corner states persist when changing the disorder patterns under weak disorder conditions, in both the nontrivial and trivial cases [figures 4(a) and 4(c)]. In these situations, the different weak disorder patterns have minimal effects on the distribution of eigenenergies, resulting in the robustness of corner states under the same degree of weak disorder, which demonstrates that these corner states are topological protected. Subsequently, we increase the disorder strength and select Type II and Type III strong disorder configurations for the two cases, respectively. Conversely, the temperature profiles measured in figures 4(b) and 4(d) clearly indicate that the bound modes still exist, but the localization positions may vary for different disorder configurations.

## 4. Conclusion

In this work, we investigate the intricate interplay between disorders and topological physics, leading to two phase transitions and the emergence of disorder-induced TAIs and AIs in heat transport. We gradually introduce onsite disorders with varying strengths to two thermal convective systems, each possessing either a trivial or nontrivial topological phase. Under weak disorder strengths, we experimentally demonstrate the induction of significant topological corner localizations in both originally nontrivial and trivial systems. These corner modes exhibit robustness against different disorder configurations, which show great potential in designing thermal meta-devices with resilience to various disorder effects [56-59]. As we increase the disorder strength further, the systems transition into AIs, where bound modes appear, but their localization positions are altered by changing the disorder profile. Our work showcases the ability to induce ordered field distributions in partially random heat transport, bridging the gap between forced well-organized systems and naturally random materials. This study challenges the conventional understanding of thermal topological physics and provides a flexible approach to control the topological phases of temperature fields. Moreover, the extension of non-Hermitian disorders into the diffusive regime suggests a distinct mechanism for manipulating other diffusive systems.

## Acknowledgements

H.G. and Z.S. acknowledge support from the Research Grants Council of Hong Kong SAR (15214323, 15200922 and 15202820). C.-W.Q. acknowledges support from the Ministry of Education, Singapore (Grant No. A-800010701-00) and the National Research Foundation, Singapore (NRF) under NRF's Medium Sized Centre: Singapore Hybrid-Integrated Next-Generation μ-Electronics (SHINE). X.Z. acknowledges support from National Natural Science Foundation of China (Grant No. 12305041) and Science and Technology Research Program of Chongqing Municipal Education Commission (Grant No. KJZD-K202300803).

## References

[1] He C, Ni X, Ge H, Sun X-C, Chen Y-B, Lu M-H, Liu X-P, and Chen Y-F 2016 *Nat.Phys.* **12**, 1124.
[2] Lu J, Qiu C, Ye L, Fan X, Ke M, Zhang F, and Liu Z 2017 *Nat.Phys.* **13**, 369.
[3] Bandres M A, Wittek S, Harari G, Parto M, Ren J, Segev M, Christodoulides D N, and Khajavikhan M 2018 *Science* **359**, eaar4005.
[4] Kraus Y E, Lahini Y, Ringel Z, Verbin M, and Zilberberg O 2012 *Phys. Rev. Lett.* **109**, 106402.
[5] St-Jean P, Goblot V, Galopin E, Lemaître A, Ozawa T, Le Gratiet L, Sagnes I, Bloch J, and Amo A 2017 *Nat. Photonics* **11**, 651.
[6] Verbin M, Zilberberg O, Kraus Y E, Lahini Y, and Silberberg Y 2013 *Phys. Rev. Lett.* **110**, 076403.
[7] Xiao M, Ma G, Yang Z, Sheng P, Zhang Z, and Chan C T 2015 *Nat.Phys.* **11**, 240.
[8] Atala M, Aidelsburger M, Barreiro J T, Abanin D, Kitagawa T, Demler E, and Bloch I 2013 *Nat.Phys.* **9**, 795.
[9] Shen S-Q, *Topological insulators* (Springer, 2012), Vol. 174.
[10] Benalcazar W A, Bernevig B A, and Hughes T L 2017 *Science* **357**, 61.
[11] Chen R, Chen C-Z, Gao J-H, Zhou B, and Xu D-H 2020 *Phys. Rev. Lett.* **124**, 036803.
[12] Kempkes S, Slot M, van Den Broeke J, Capiod P, Benalcazar W, Vanmaekelbergh D, Bercioux D, Swart I, and Morais Smith C 2019 *Nat. Mater.* **18**, 1292.
[13] Peterson C W, Benalcazar W A, Hughes T L, and Bahl G 2018 *Nature* **555**, 346.
[14] Schindler F, Cook A M, Vergniory M G, Wang Z, Parkin S S, Bernevig B A, and Neupert T 2018 *Sci. Adv.* **4**, eaat0346.
[15] Xue H, Yang Y, Gao F, Chong Y, and Zhang B 2019 *Nat. Mater.* **18**, 108.
[16] Qi Y, Qiu C, Xiao M, He H, Ke M, and Liu Z 2020 *Phys. Rev. Lett.* **124**, 206601.
[17] Yang Y, Gao Z, Xue H, Zhang L, He M, Yang Z, Singh R, Chong Y, Zhang B, and Chen H 2019 *Nature* **565**, 622.
[18] Tao Y-L, Yan M, Peng M, Wei Q, Cui Z, Yang S A, Chen G, and Xu Y 2024 *Phys. Rev. B* **109**, 134107.
[19] Wang J-H, Yang Y-B, Dai N, and Xu Y 2021 *Phys. Rev. Lett.* **126**, 206404.
[20] Anderson P W 1958 *Phys. Rev.* **109**, 1492.

[21] Li J, Chu R-L, Jain J K, and Shen S-Q 2009 *Phys. Rev. Lett.* **102**, 136806.
[22] Groth C, Wimmer M, Akhmerov A, Tworzydło J, and Beenakker C 2009 *Phys. Rev. Lett.* **103**, 196805.
[23] Guo H-M, Rosenberg G, Refael G, and Franz M 2010 *Phys. Rev. Lett.***105**, 216601.
[24] Li C-A, Fu B, Hu Z-A, Li J, and Shen S-Q 2020 *Phys. Rev. Lett.* **125**, 166801.
[25] Yang Y-B, Li K, Duan L-M, and Xu Y 2021 *Phys. Rev. B* **103**, 085408.
[26] Meier E J, An F A, Dauphin A, Maffei M, Massignan P, Hughes T L, and Gadway B 2018 *Science* **362**, 929.
[27] Zhang W, Zou D, Pei Q, He W, Bao J, Sun H, and Zhang X 2021 *Phys. Rev. Lett.* **126**, 146802.
[28] Stützer S, Plotnik Y, Lumer Y, Titum P, Lindner N H, Segev M, Rechtsman M C, and Szameit A 2018 *Nature* **560**, 461.
[29] Liu G-G, Yang Y, Ren X, Xue H, Lin X, Hu Y-H, Sun H-x, Peng B, Zhou P, and Chong Y 2020 *Phys. Rev. Lett.* **125**, 133603.
[30] Zangeneh-Nejad F and Fleury R 2020 *Adv. Mater.* **32**, 2001034.
[31] Liu H, Xie B, Wang H, Liu W, Li Z, Cheng H, Tian J, Liu Z, and Chen S 2023 *Phys. Rev. B* **108**, L161410.
[32] Zhang D-W, Tang L-Z, Lang L-J, Yan H, and Zhu S-L 2020 *Sci. China: Phys. Mech. Astron.* **63**, 267062.
[33] Tang L-Z, Zhang L-F, Zhang G-Q, and Zhang D-W 2020 *Phys. Rev. A* **101**, 063612.
[34] Wu H and An J-H 2020 *Phys. Rev. B* **102**, 041119.
[35] Wang R, Zhang K, and Song Z 2021 *J. Phys. Commun.* **5**, 095011.
[36] Liu H, Zhou J-K, Wu B-L, Zhang Z-Q, and Jiang H 2021 *Phys. Rev. B* **103**, 224203.
[37] Lin Q, Li T, Xiao L, Wang K, Yi W, and Xue P 2022 *Nat. Commun.* **13**, 3229.
[38] Mo Q, Sun Y, Li J, Ruan Z, and Yang Z 2022 *Phys. Rev. Applied* **18**, 064079.
[39] Gu Z, Gao H, Xue H, Wang D, Guo J, Su Z, Zhang B, and Zhu J 2023 *Sci. China: Phys. Mech. Astron.* **66**, 294311.
[40] Cao P, Li Y, Peng Y, Qiu C, and Zhu X 2019 *ES Energy & Environment* **7**, 48.
[41] Li Y, Peng Y-G, Han L, Miri M-A, Li W, Xiao M, Zhu X-F, Zhao J, Alù A, and Fan S 2019 *Science* **364**, 170.
[42] Gao H, Xue H, Gu Z, Liu T, Zhu J, and Zhang B 2021 *Nat. Commun.* **12**, 1888.
[43] Gao H, Xue H, Wang Q, Gu Z, Liu T, Zhu J, and Zhang B 2020 *Phys. Rev. B* **101**, 180303.
[44] Lin Q, Li T, Xiao L, Wang K, Yi W, and Xue P 2022 *Phys. Rev. Lett.* **129**, 113601.
[45] Liu S, Ma S, Yang C, Zhang L, Gao W, Xiang Y J, Cui T J, and Zhang S 2020 *Phys. Rev. Applied* **13**, 014047.
[46] Wang W, Wang X, and Ma G 2022 *Nature* **608**, 50.
[47] Zeng Q-B, Yang Y-B, and Xu Y 2020 *Phys. Rev. B* **101**, 020201.
[48] Zhao H, Qiao X, Wu T, Midya B, Longhi S, and Feng L 2019 *Science* **365**, 1163.
[49] Xu G, Zhou X, Li Y, Cao Q, Chen W, Xiao Y, Yang L, and Qiu C-W 2023 *Phys. Rev. Lett.* **130**, 266303.
[50] Xu G, Li W, Zhou X, Li H, Li Y, Fan S, Zhang S, Christodoulides D N, and Qiu C-W 2022 *Proc. Natl. Acad. Sci.* **119**, e2110018119.
[51] Qi M, Wang D, Cao P C, Zhu X F, Qiu C W, Chen H, and Li Y 2022 *Adv. Mater.* **34**, 2202241.
[52] Xu G, Yang Y, Zhou X, Chen H, Alu A, and Qiu C-W 2022 *Nat. Phys.* **18**, 450.
[53] Xu G, Zhou X, Yang S, Wu J, and Qiu C-W 2023 *Nat. Commun.* **14**, 3252.
[54] Wu H, Hu H, Wang X, Xu Z, Zhang B, Wang Q J, Zheng Y, Zhang J, Cui T J, and Luo Y 2023 *Adv. Mater.* **35**, 2210825.
[55] Li A, Xu B, and Xie B 2024 *arXiv preprint arXiv:2404.15088*.
[56] Fan C, Gao Y, and Huang J 2008 *Appl. Phys. Lett.* **92**.
[57] Liu Z, Cao P-C, Xu L, Xu G, Li Y, and Huang J 2024 *Phys. Rev. Lett.* **132**, 176302.
[58] Yang F, Zhang Z, Xu L, Liu Z, Jin P, Zhuang P, Lei M, Liu J, Jiang J-H, and Ouyang X 2024 *Rev. Mod. Phys.* **96**, 015002.
[59] Zhang Z, Xu L, Qu T, Lei M, Lin Z-K, Ouyang X, Jiang J-H, and Huang J 2023 *Nat. Rev. Phys.* **5**, 218.